Applied Chemical Engineering (2026) Volume 9 Issue 3 ISSN: 2578-2010 (O)
doi: 10.59429/ace.v9i3.5954

RESEARCH ARTICLE

Influence of Fe3O4 ferrofluid medium Viscosity on local hyperthermic response for Cancer Therapy

Maan Al-Nuaim*[1], Hashim Jabbar[2], Sumaia H. Gatia[3], N. A. Abdullah[4]

[1] *Department of Pharmaceutical Chemistry, College of Pharmacy, University of Basrah, Iraq*

[2,3,4] *Department of Physics, College of Science, University of Basrah, Iraq*

***Corresponding author:** Maan Al-Nuaim, maan.suwaid@uobasrah.edu.iq*

ABSTRACT

The fields of biotechnology and medicine are significantly impacted by the development of nanotechnology and associated materials. Presently, a prominent subject in life sciences and healthcare is the application of magnetic nanoparticles (MNPs) owing to their size-variable physical and chemical characteristics. Specifically, nanoparticles of iron oxide are being extensively studied to cure magnetic hyperthermia and provide very effective cancerous cell death. In this work, ferric and ferrous chloride were used as the starting precursors in coprecipitation process for producing magnetic Fe3O4 (NPs). Dynamic Light Scattering (DLS), Transmission Electron Microscopy, Field Emission Scanning Electron Microscopy (FE-SEM), Powder X-ray Diffraction (XRD), Fourier Transform Infrared Spectroscopy (FTIR), and Vibrating Sample Magnetometer were utilized to analyze the produced NPs. The results revealed that the NPs have spinal structure with a consistent size and a spherical shape. According to the magnetic data, sample has a soft hysteresis loop, demonstrating their ferrimagnetic nature. Furthermore, compared to the water medium, the magneto thermal response of Fe3O4 distributed in water/glycerol mixture exhibited 37% higher heat induction. These results highlights the importance of the medium viscosity in heat induction and medium of blood viscosity enhances the quantity of heat delivered, which is very promising result in hyperthermia for cancer therapy.

Keywords: Fe3O4 nanoparticles; Co-precipitation; Ferrofluid; Viscosity; Magnetic hyperthermia; Cancer therapy.

ARTICLE INFO

Received: 23 March 2026
Accepted: 25 June 2026
Available online: 1 July 2026

1. Introduction

The majority of human cancers remain incurable despite decades of intensive research and several treatment trials. There are several factors at play here. a number of multiple causes and forms of "cancer." Each one is unique and reacts to treatments in a distinctive way. Lack of knowledge about the processes behind tumor growth and therapeutic intervention are the main limiting constraints. Although certain neoplasms have been successfully treated [1,2], many tumor forms are resistant to contemporary treatments [3]. The three main cancer treatment modalities during the last few decades have been chemotherapy, radiation therapy, and surgery. Although they have had some success, other methods like therapeutic hyperthermia are not yet regarded as standard-of-care treatments.

In the medical and biological sciences, nanoparticles are arguably the most common type of nanomaterial. Materials with size-dependent physical, chemical, and biological characteristics that are notably distinct are found when particle sizes are decreased to the nanoscale. One of the most useful applications of nanoparticles in medicine is the control and use of their magnetic characteristics, which may be used

for the detection and treatment of cancer. The research involves the design, synthesis, and analysis of a wide variety of unconventional magnetic nanoparticles and core-shell nanostructures. Magnetic nanoparticles demonstrate many practical uses, including imaging with magnetic resonance, hyperthermia, method of separation or drug delivery, and catalytic, contingent upon their size, content, structure, and physicochemical properties [4-9].

Currently, the foundation of interdisciplinary approaches to the problem is the construction of multifunctional nanoparticles that may satisfy several criteria for a particular application. The creation of multifunctional magnetic nanoparticles with the maximum saturation magnetization and appropriately functionalized surfaces that enable them to bind to target cells or tissues selectively is one of the primary objectives in the context of biomedical applications. [10]. To get this highly desired selectivity, DNA probes, immune system antibodies and various chemical entities are commonly utilized [11]. Colloidal iron oxides and also iron oxide-derived core-shell the nanostructures have garnered significant interest for a variety of Utilizations [12]. Other considerations like biocompatibility or toxicity must be made, even though there are other materials that better fulfill the magnetic requirements for biological applications (i.e., materials exhibiting increased saturation magnetization). Iron oxides are good prospects for use in biomedical applications and in-vivo investigations since they are believed to be non-toxic and biocompatible, in addition to having intriguing size-dependent magnetic characteristics and the capacity for functionalization using both organic and inorganic substances chemicals [13].

Recently, magnetic nanoparticles heated with alternating magnetic fields have been employed as a potential cancer treatment to produce hyperthermia targeted directly at cancer cells [14-19]. Superparamagnetic NP in a magnetic fluid experience abrupt changes in magnetization direction when subjected to a high-frequency alternating field of magnetism. When an external magnetic field is applied, the nanoparticles' magnetic moments align with the field's direction. The Brownian or Néel relaxation method, which is connected with the extravagance of potential energy into surroundings particulate matter describes how magnetic nanoparticles attain an equilibrium state when the magnetic field is deactivated [20-23]. With a typical relaxation period τ_B in the series of microseconds, the Brownian relaxation procedure occurs when the whole particle spins in the nearby fluid. It may be described as follows:

$$\tau_B = \frac{3V_H\eta}{k_BT} \quad (1)$$

where η is the dynamic viscosity of the surrounding liquid, V_H is the magnetic particle's hydrodynamic volume, T is the absolute temperature, and k_B is Boltzmann's constant ($1.38 \times 10-23\,JK^{-1}$). The rotating drag in the surrounding fluid creates an energy barrier for the reorientation of particles. Since heat creation results from viscous friction between the oscillating particles and the neighboring middling, losses caused by the Brownian process are also known as viscous losses. Superparamagnetic particles are not the only particles that experience this kind of loss.

Generally, in the presence of a fluctuating magnetic field H, particles having residual magnetic fields (M_r) that may be thought of as tiny permanent magnets experience a torque $T = \mu_O M_r H_V$. In the state of equilibrium, the magnetic torque T is affected by the viscous resistance of fluid, $12\pi\eta Vf$, and the loop deprivation energy is determined by $2\pi T$ [24]. The mechanism described, referred to as Néel relaxation [25], employs an external AC magnetic field to facilitate the rotation of the magnetization vector within the particle's magnetic core, enabling it to overcome the energy barrier E = KV, where V represents the particle volume and K denotes the particle's anisotropy constant. The probability of this transition is given by exp(σ), where σ denotes the ratio of anisotropy energy to thermal energy, expressed as KV/k_B T. The relaxation duration τ_N of the magnetic nanoparticles while Néel release is characterized by a defined formula, with potential values spanning from milliseconds (and as many as nanoseconds) to a few seconds:

$$\tau_N = \tau_O \cdot exp(\sigma) = \tau_O \cdot exp\left(\frac{KV}{k_B T}\right) \quad (2)$$

Where τ_O is the damping or decay period (about $10^{-8} - 10^{-10}$ s), the following formulae are for both high and low energy barrier values:

$$\begin{aligned} \tau_N &= \tau_O \cdot \sigma^{-\frac{1}{2}} \cdot exp(\sigma), \ \sigma > 2 \\ &= \tau_O \cdot \sigma, \qquad \sigma << 1. \end{aligned} \quad (3)$$

The dispersion of particle sizes results in a range of relaxation periods, with both relaxation processes influencing magnetization. The term real relaxation time is thereby generated, applicable to particular particles:

$$\tau_{eff} = \tau_N \cdot \frac{\tau_B}{\tau_B + \tau_N} \quad (4)$$

The predominant mechanism is defined by its shortest period of relaxation [21,25]. The metric known as "Specific Absorption Rate" (SAR) is commonly utilized to quantify the magnetic heating capacity of magnetic nanoparticles when subjected to an oscillating magnetic field. The specific absorption rate (SAR), measured in watts, indicates the amount of heating power (P) generated per unit mass of the magnetic component of the sample (m_MNP), expressed in grams [26]:

$$SAR = \frac{P}{m_{MNP}} \quad (5)$$

Numerous factors, including particle size and shape, concentration, magnetic permeability (μ), the intensity of the magnetic field (H), frequency (f), and viscosity of the sample, affect SAR. These factors can be influenced by the physical-chemical characteristics of the material under investigation or by the technique used to apply the high-frequency magnetic field [27,28]. Skumiel et al.'s study [29] analyzed the thermal characteristics of oil-based magnetic fluids with variations in concentration of magnetic particles. The SAR value was greater in the samples with a lower magnetite volume proportion. Applying rotating [30] and alternating [31] magnetic fields produced comparable results. In the later situations, the thermal impact was obviously concentration-dependent and included agar gel-suspended magnetite nanoparticles. The viscosity was around 100 mPa·s for samples with a 7% agar content, which was many times more than that of magnetic liquids. Despite the high viscosity coefficient in agar samples, the thermal effect's power loss study revealed that both processes (Néel and Brown) were responsible for losses. Additionally, it was demonstrated that the thermal impact, as approximated using Equation (5), decreased as the magnetite concentration increased (i.e., as the distances between NPs decreased). Larger interactions between NPs can explain this. Aggregate development in increasingly concentrated magnetic fluids is the cause of this. Viscosity has significance when the parameters are kept constant, including the kind, size, and concentration of magnetic nanoparticles as well as the application circumstances (H, f). Actually, the methodology's fundamental goal to keep all parameters of the experiment and samples at a consistent. Under these circumstances, the main goal is to investigate how viscosity—which is influenced by different kinds of carrier liquid—affects heat dissipation during an experiment in a high-frequency alternating the field of magnetic. Changes in rheological (viscosity) characteristics are associated with shifts in the distribution of magnetic particle sizes in magnetic fluid. By changing the particles' magnetic moment, it modifies the intensity of magnetic interactions, which in turn influences how aggregates form in the magnetic fluid [32]. As was already established, viscosity is able to considerably affect the magnetic relaxation processes. By altering the viscosity, writers have attempted to differentiate between how heating is affected by Brownian and Neel relaxation in a number of studies. Comparative SAR studies were also carried out for agar-based phantom samples and magnetosome suspension[33]. The limiting of Brownian motion caused a discernible drop in heating efficiency when magnetosomes were positioned in a gel structure. Eirini Myrovali et al. conducted a study on heat induction in

relation to medium viscosity, examining the different methods of heat generation, including Brownian motion, Néel relaxation, and hysteresis losses, across various sizes. The separation of Brownian and hysteresis losses was conducted to determine optimal values. They demonstrated that, for low viscosities, the heating in range is equally attributed to hysteresis and Brownian losses. In stiff media, however, hysteresis losses continue to be the primary source of heat, whereas Brownian losses progressively diminish as medium viscosity does [34]. Cabrera et al. [35] examined the specific absorption rate (SAR) values of iron oxide nanoparticles suspended in agar and water. SAR values in both water and the agar were similar at low doses (3 mg Fe3O4·mL^(-1)), but at a concentration of (10 mg Fe3O4·mL^(-1)), the SAR levels in water were twice those in agar. Interparticle interaction activities that enhance heat generation were linked to the rise of values for SAR observed in water at higher particle concentrations.

The aim of this study is to analyze the variations in SAR and heat induction between two magnetic fluids with two distinct viscosities. Investigations were conducted on ferrofluids composed of water and a mixture of 60% water and 40% glycerol, which is equivalent to the viscosity of human blood. It is crucial to comprehend how viscosity affects heat dissipation in these fluids because of their potential applications biomedicine as a therapeutic instrument for magnetic hyperthermia, where fluids of differing viscosities may serve as model materials to better understand heat evolution under specific circumstances.

2. Fe3O4 synthesis and characterizations

Magnetite NPs were produced via co-precipitation at about 25 °C utilizing of water-based mixtures of Fe^{3+} and Fe^{2+} ions in addition to a concentrated NH4OH solution (32%). The pH of the solution was adjusted to pH=12 with a constant stirring for 20 min. A black substance precipitated from a solution or stabilized magnetic NPs were obtained by removing precipitation reaction byproducts using magnetic decantation. Then the produced black MNPs repeatedly subjected to deionized water and ethanol rinse processes. Following that, the magnetic nanoparticles were spread out at (50-55 °*C*) in a nonpolar liquid carrier. To create a nonpolar magnetic fluid, the magnetic NPs underwent flocculation, redispersion, and magnetic decantation/filtration.

Several methods were used to characterize the produced MNPs. X-ray diffractometer (XRD; Philips, model X'Pert Pro) was used to do the XRD investigation of magnetite NPs using a Cu Kα source ($\lambda = 1.54056$ Å).

The Fourier-transform infrared spectroscopy (FTIR) was utilized to verify the structure and binding of magnetite NPs. The Perkin-Elmer spectrum (BX spectrometer) was employed to acquire FT-IR spectra at room temperature (RT) over the series of (400-4000 cm cm^{-1}) with a resolution of spectral of 4 cm^{-1}.

A transmission electron microscope that uses field emission to achieve high resolution (FE-SEM; MIRA3 TESCAN) was utilized to examine the morphology, dimensions, microstructure, and distributions of the MNPs in the NP sample. For optimal imaging, the samples were coated with gold via sputtering, a conductive material, to produce the MNPs. The constituent content and analysis of elemental rate or the particles composition was ascertained using energy dispersive spectroscopy (EDS). Using a (SZ-100z Dynamic Light Scattering and Zeta Potential Analyzer, Manufacturer: Horiba Jobin Yvon) device, the hydrodynamic size distribution of the particles in the watery solution was ascertained.

Using a sample magnetometer that vibrates (MDK-VSM-University of Basrah) at ambient temperature and within a field of magnets of up to 1.4 T, *M-H* loop measurements were carried out on the Fe3O4 NPs powders at RT.

The *T* vs. *t* dependency in an alternating magnetic field (AMF) was measured in order to determine hyperthermic characteristics, especially the heating rate, *dT*/*dt*, and the exact loss power *SLP*. The (MDK-HyperThermia -University of Basrah) device's LC circuit is operated by a generator of alternating voltage with frequency *f* and voltage V. A magnetic field can be generated, the coil raises the temperature of the liquid by

altering the magnetization of MNPs (for more details, see Supplementary Materials). A 400 *kHz* frequency and in the form of an amplitude-modulated alternating magnetic field ranging from 50 to 400 Oe were used for the measurements. In order to remove any potential inaccuracies brought on due to parasitic thermal effects in the carrier fluid, the glass vial carrying the sample was isolated from the coil wrapping with running water that has been cooled and differential temperature measurements. The thermometer's fitted probe is insensitive to alternating magnetic fields.

3. Results and discussions

Several characterization have been done for the surface such as Transmission Electron Microscopy (TEM), Vibrating Sample Magnetometer (VSM), X-ray diffraction pattern (XRD), FTIR spectra, SEM and EDX

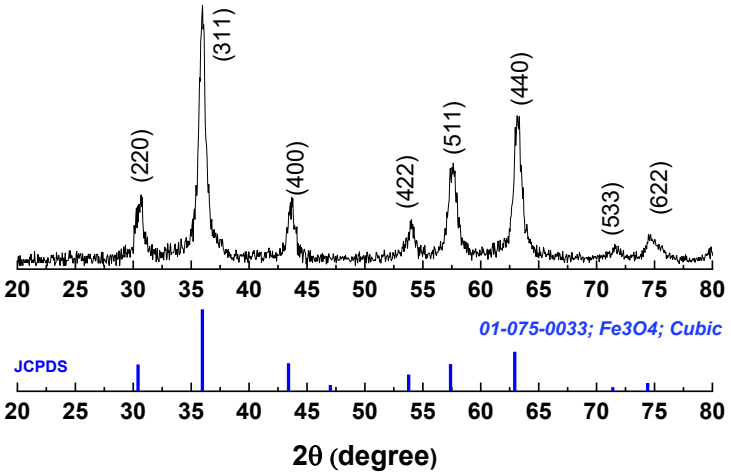

Figure 1. The X-ray diffraction pattern of Fe3O4 NPs. produced via the co-precipitation technique (top panel). Bottom panel represents the standard XRD pattern as per JCPDS card of the structure.

Fig. 1 displays the XRD patterns of NPs sample, demonstrating the crystalline nature of these particles. Magnetite (Fe3O4) (2Θ = 30.42°, 35.96°,43.4°, 53.78°, 57. 38°, 62.93°, 71.4°, 74.41°) was found to have a number of distinctive peaks that corresponded to the crystal planes of (220), (311), (400), (422), (511), (440), (533), and (622), in that order. These peaks correspond with the magnetite phase ((JCPDS card no. 01-075-0033; Fe3O4; Cubic spinal structure) [36] standard data. Using the Debye-Scherrer equation, The mean size of the crystallites was determined to be 12.14 nm. The manufactured sample broad reflections show that magnetite is a nanocrystalline material. This indicates the generation of Fe3 O4 NPs in this work with no goethite structure (FeOOH), which corresponds to the (110) plane, in which the little peak that can be seen at 2θ = 24.17° along with two more peaks in the XRD pattern linked to the goethite phase, which are situated at 24.17° and 33.12° (211) and (100) [37].

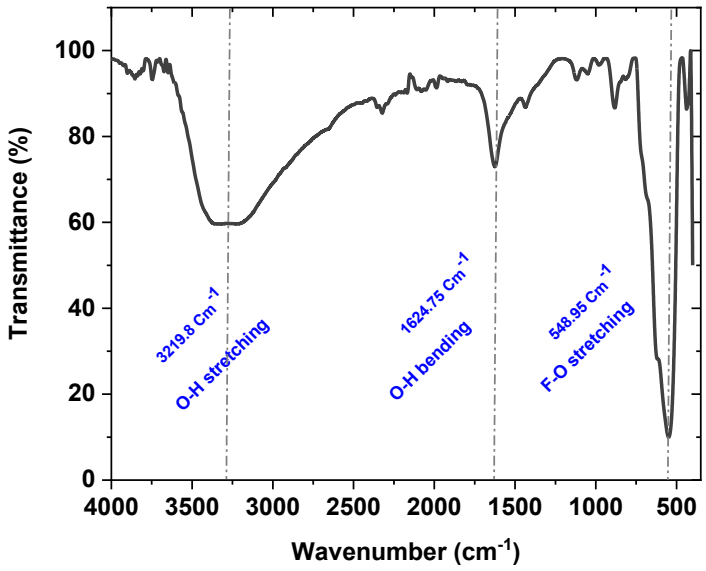

Figure 2. FTIR spectra of unadulterated magnetite NPs produced by co-precipitation approach (the main absorption peaks indicated by the dashed lines).

The Fe3O4 FTIR spectrum is shown in Fig. 2. The primary magnetite characteristic phase is reliably distinguished using FTIR spectroscopy. The characteristic strong band at 548.9 cm^{-1} confirms the magnetite phase's presence, but unique bands of the magnetite phase (γ-Fe2O3) in the $740 - 620\ cm^{-1}$ spectral range are not present. This outcome demonstrates that our approach enables the synthesis of the single magnetite phase even when the heterometallic precursor is present. The O-H stretching vibration can be observed by the bands close to 3219.8 cm^{-1} and 1624.75 cm^{-1}[38-40].

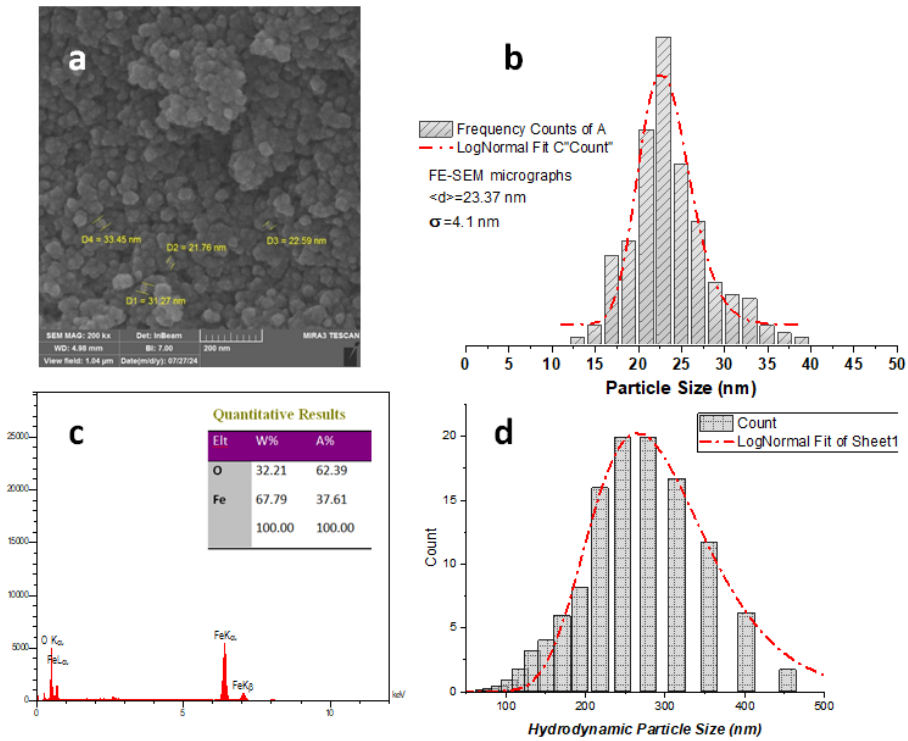

Figure 3. FESEM image Fe3O4 MNP sample (b) MNP grain size distribution histograms fitted by LogNormal function based on FESEM micrographs, (c) EDS spectrum (the corresponding elemental analysis is presented in top-right insets), (d) DLS particle hydrodynamic size distributions for Fe3O4 MNP sample fitted by LogNormal function.

The surface morphology of the Fe3O4 NPs by FESEM image is depicted in Fig.3a. These show that the Fe3O4 NPs were mostly spherical particles with sizes between 10 and 40 nm. Fe3O4 particles exhibit some aggregation, as seen in Fig 3b the relatively broad size distribution of values with an average particle size of $23.37nm$ and standard deviation of $4.1\ nm$ Although these agglomerations are often identified as a results of interparticle magnetic force or overlapping fragments kept together through weak Van der Waals forces [41], they are typically generated by the absence of a capping agent in the nanoparticle production process [42]. The samples' chemical compositions were examined using the EDX method. The EDX spectrum of Fe3O4 NPs is seen in Fig.3c, confirming the compound iron and oxygen element contents. While no other elements were present as a trace, the iron of (62.39%) and oxygen of (37.61%) were noted in the total weight of the Fe3O4 NPs.

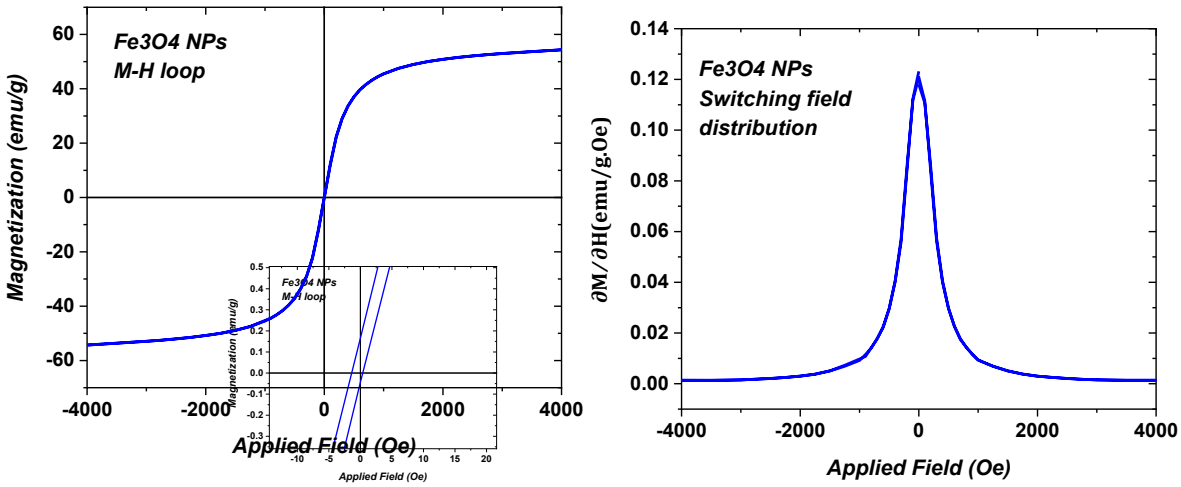

Figure 4. (left panel) magnetization at RT as a result of the magnetic field applied (inset a zoom in image showing Hc), (right panel) the first deverative of magnetization which represents the switching field distribution.

Left panel of Fig. 4 displays the magnetization dependencies that were obtained at RT in relation to the magnetic field that was used. Inset of Fig 4 revealed that sample exhibit soft hysteresis behavior or very little coercive field ($H_C = 0.85\ Oe$) with a saturation magnetization value of around ($M_S = 54.5\ emug^{-1}$), according to the observed dependence. Naturally, the saturation magnetization values ($\sim 54.5\ emu \cdot g^{-1}$) that were observed for Fe3O4 nanoparticles were different compared to those documented for their bulk equivalents ($92 - 100\ emug^{-1}$) and typically declined with size ($\sim 88\ emu \cdot g^{-1}$) [43,44]. Size effect and superparamagnetic fractions normally contribute to the lower magnetic saturation.

Fig. 5 schematically depicts the (MDK-hyperthermia) AC magnetic field energy dissipation setup. A cylindrical water-cooled solenoid-type inductor powered by a 20 kW electronic generator produces a magnetic field of up to 40 mT. A field inductor, a glass tube container holding a liquid sample (see Fig. 5 b), and a precise and sensitive temperature sensor are positioned in the upper portion of the apparatus. A sensor coil for magnetic field control is positioned in the lower section. Measurements, data collection, and experiment management are all done using a computer system.

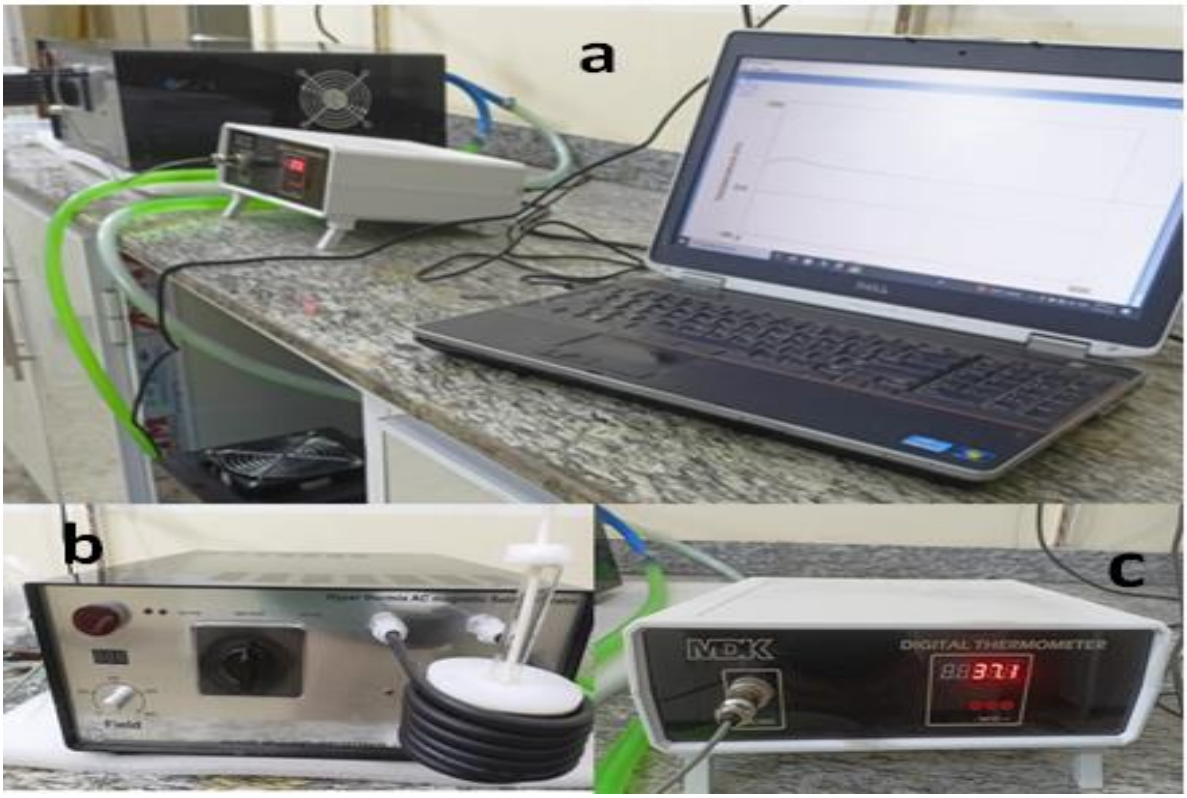

Figure 5. Photos represent the components of (MDK-hyperthermia) setup used for calorimetric measurements in this study.

Heat dissipation studies on dispersion samples in low viscosity (water medium) and higher viscosity (water+glycerol medium) are illustrated in Fig. 6. The sample dispersed in a medium with a viscosity similar to human blood had a much higher heat rate than the sample with a lower viscosity. The heat rate ($\Delta T/\Delta t$) value of sample $10\ mg/mL$ of Fe3O4 NPs dispersed in high viscosity medium was 40% larger. These results indicate the powerful Brownian mechanism capacity to produce heat. The two curves in Fig. 6 reveals that the system temperature increase of both medium viscosities of magnetite ferrofluids with concentrations of 10 mg/mL and f=400 KHz. Depending on the amount of medium viscosity, the samples with Fe3O4 NPs in mixture exhibited a temperature increase of 15 degrees after being exposed to an AC magnetic field for 120 seconds, while for water medium the rise is about 9 degree. The systems cooling curves encompass a duration range of *120* to *600* s.

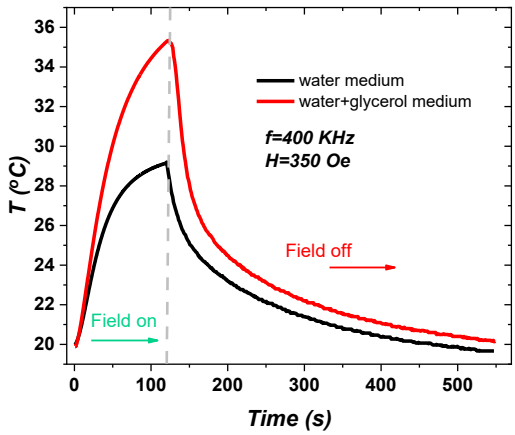

Figure 6. (field on) The rise in temperature of the two medium viscosities of Fe3O4 NPs till 120 s. (field off) The cooling curves of the systems span a time interval of 120 to 600s.

The calorimetric results of suspensions of $10\,mg/mL$ Fe3O4 NPs in two medium viscosities with a frequency fixed at $400\,kHz$ are presented in Fig. 7. The right panel shows the heat induced in water+glycerol medium, the left panel shows the effect in water medium. A time-dependent, progressive rise in the temperature of the two aqueous solution under AC-MF was noted in the induction heating trials for the two systems at an applied AC-MF of (100 to $400\,Oe$). The heat generated in the water+glycerol media is obviously more than that in the water medium. An induction heating device was used to track the time-related magnetic heating efficacy of $1\,ml$ aqueous solutions of Fe3O4 NPs (in microcentrifuge tubes).

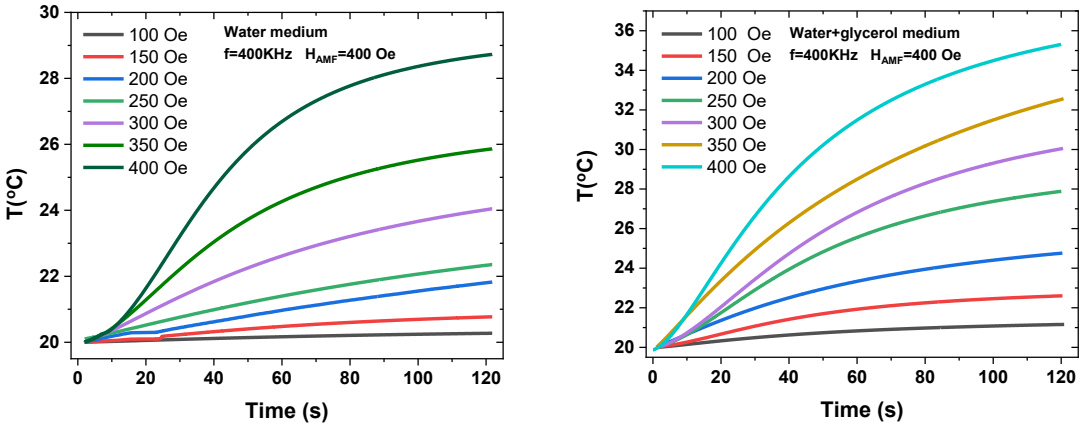

Figure 7. (*T-t*) Measurements curves conducted at varying AMF field amplitude with frequency were set to 400 *kHz*. Left panel represents the water medium while the right one for water+glycerol medium.

The fixed ambient temperature was $20\,°C$ for all measurements. For every surface where losses of radiation occur, the surface emissivity was set to 1. Nevertheless, as the temperature change is often small, these losses may typically be disregarded. The magnetic field strength, which fluctuates along the coil's axis, determines the power generation rate. Equation was used to calculate the power distribution in the axial direction (5). The average rate of temperature change (i.e. $\Delta T/\Delta t$) throughout a 120 second period was then used to compute the SLP derived from predicted temperature increase throughout time. The warmest area of the sample, which was discovered to be close to the upper surface of the fluid, was invariably where the temperature data was taken. The following formula was used to get the specific absorption power (SLP), which is typically used to indicate heating efficiency [45,46]:

$$SLP = C_S(\frac{\Delta T}{\Delta t})\frac{M_{Sol.}}{M_{MNPs}} \tag{6}$$

where $(\Delta T/\Delta t)$ is the pace of the temperature curve with time and C is the solvent's specific heat ($C_S = C_{water} = 4.18\,J/g\,°C$), ($C_S = C_{blood} = 3.617\,J/g\,°C$), M_{Sol} and $MMNPs$ are the masses of the solvent and $MNPs$ used for measurement.

With assume the sample temperatures is constant and the losses of heat are minimal throughout a specific time period of the heating process, the entire curve was utilized for SLP calculation. Additionally, regardless of the curve fitting techniques used, it is demonstrated that a larger error occurs when calculating the initial temperature slope with a higher power level and longer time to heat. For this reason, a higher order curve fitting (such as two polynomial and exponential) is preferred as heating duration or power density rises. Furthermore, the SLP is unaffected by the sample shape when the magnetization of a suspension of nanoparticles is minimal [47, 48].

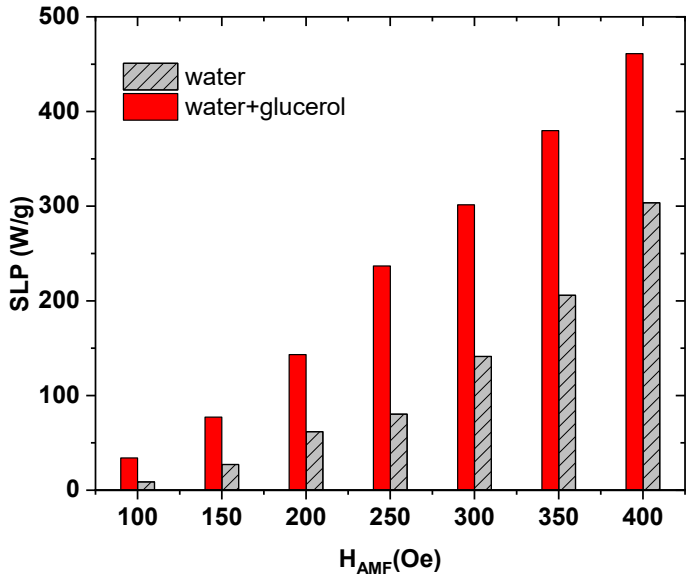

Figure 8. SLP dependency of the amplitude of the magnetic field strength for the two distinct viscosity systems at a given frequency of 400 KHz and a medium concentration of 10 mg/mL.

The thermal energy generated by these two suspending via Néel relaxation (reorientation of magnetic spins) and Brownian relaxation (rotation of particles) loss mechanisms is sufficiently capable of elevating the temperature of 10 mg of Fe3O4 NPs /ml suspending to the temperature of hyperthermia range (42–43 °C), taken into account human body temperature even under an applied AC-MF (H_{AMF}) lower than maximum field. This remains within the acceptable limits of frequency and field strength as indicated by Hergt and Dutz [49] for the Using hyperthermia safely in patients ($H_{AMF} \times f$ should be less than $5 \times 10^9\ Am^{-1}\ s^{-1}$) [49].

The above results of SLP and temperature increase in both media showed 37% larger SLP in mixture medium which is often rather tolerable, particularly in blood-like viscous systems where some investigations produced contradictory results that rely on the morphology, magnetism, and intermediate characteristics of the nanoparticles. Bhardwaj et al. calorimetric results analysis on a water and agarose gel phantom system demonstrated that, for the Mn1−xZnxFe2O4 sample with the lowest concentration, it is feasible to control the hyperthermia temperature at lower fields and frequencies, which can be suitable for in vitro research [50]. Andrade et al. found that without coating nanoparticles efficiently distribute heat through both Néel and Brown relaxation processes when suspended in low viscosity liquids (water, triethanolamine, and ethylene glycol) under an applying oscillation field of magnets, resulting in a temperature increase of approximately 21 °C. Heat dissipation is preferentially controlled by the Néel relaxation of the magnetization since the silica layers tend to prevent the Brownian motion of coated particles [51]. In water medium, Tong et al. calculated SLP of $1026\ W/g$ using a frequency value of $325\ kHz$ [52]. Similarly, if sample Fe3O4 had f value of $300\ kHz$. This computation demonstrated that the resulting MNPs would undoubtedly be capable of producing such SLP value in the kHz range. Cervadoro et al. employed a rate of recurrence series of 0.2 to $30\ MHz$ in a related study [53]. The frequencies employed for MHT applications usually fall between 100 kHz to 300 kHz, which is the range of safe in vivo (application inside of the body of human) [54-57].

4. Conclusions

In summary, the simple and inexpensive chemical coprecipitation method was used to produce magnetite NPs which is confirmed by FTIR spectrum. The XRD examination demonstrated the spinal magnetite structure of 12.41 nm crystallite size. Nearly spherical-like nanoparticles (NPs) with mean sizes of 23.37 nm were estimated from FESEM images. According to DLS particle size distributions, Fe3O4 NPs have a

hydrodynamic dimensions of 200 nm. The results of the hysteresis loop showed that although the M_S values are rather significant, the H_C values are extremely small. Furthermore, the VSM loop analysis confirmed the hysteresis loop results, pointing to the Fe3O4 NPs SP proportions of sample ferrimagnetic nature is demonstrated. Additionally, the magneto thermal response of Fe3O4 dispersed in a water/glycerol combination showed 37% greater heat induction than the water medium. These results demonstrate the significance of medium blood viscosity in heat induction and the fact that it increases the amount of heat supplied, both of which are highly promising outcomes for cancer treatment-induced hyperthermia.

Acknowledgements

The authors express their gratitude to the team at MDK Company and the Department of Physics at the University of Kashan for their valuable support.

Funding

Financed by the University of Basrah.

Conflicts of interest/Competing interests

The authors wish to affirm that there are no conflicts of interest to disclose.

Data and code availability

Upon reasonable request, the data will be made available.

Ethical approval

Not Applicable.

References

1. Tallman MS, Andersen JW, Schiffer CA, Appelbaum FR, Feusner JH, Ogden A, Shepherd L, Willman C, Bloomfield CD, Rowe JM, Wiernik PH. All-trans-retinoic acid in acute promyelocytic leukemia. N Engl J Med. 1997 Oct 9;337(15):1021-8. doi: 10.1056/NEJM199710093371501.
2. Pui CH, Robison LL, Look AT. Acute lymphoblastic leukaemia. Lancet. 2008 Mar 22;371(9617):1030-43. doi: 10.1016/S0140-6736(08)60457-2.
3. Jemal A, Siegel R, Ward E, Hao Y, Xu J, Murray T, Thun MJ. Cancer statistics, 2008. CA Cancer J Clin. 2008 Mar-Apr;58(2):71-96. doi: 10.3322/CA.2007.0010. Epub 2008 Feb 20.
4. Myrovali, E. Hybrid Stents Based on Magnetic Hydrogels for Biomedical Applications. ACS Appl. Bio Mater. 2022, 5, 2598, DOI: 10.1021/acsabm.2c00088
5. Bray F, Laversanne M, Sung H, Ferlay J, Siegel RL, Soerjomataram I, Jemal A. Global cancer statistics 2022: GLOBOCAN estimates of incidence and mortality worldwide for 36 cancers in 185 countries. CA Cancer J Clin. 2024 May-Jun;74(3):229-263. doi: 10.3322/caac.21834. Epub 2024 Apr 4.
6. Wan Mohd Zawawi WFA, Hibma MH, Salim MI, Jemon K. Hyperthermia by near infrared radiation induced immune cells activation and infiltration in breast tumor. Sci Rep. 2021 May 13;11(1):10278. doi: 10.1038/s41598-021-89740-0
7. Pankhurst, Quentin A., et al. "Applications of magnetic nanoparticles in biomedicine." Journal of physics D: Applied physics 36.13 (2003): R167.
8. Laurent, Sophie, et al. "Magnetic iron oxide nanoparticles: synthesis, stabilization, vectorization, physicochemical characterizations, and biological applications." Chemical reviews 108.6 (2008): 2064-2110.
9. Hadjipanayis, Costas G., et al. "Metallic iron nanoparticles for MRI contrast enhancement and local hyperthermia." Small (Weinheim an der Bergstrasse, Germany) 4.11 (2008): 1925.
10. Yoo, Dongwon, et al. "Theranostic magnetic nanoparticles." Accounts of chemical research 44.10 (2011): 863-874.
11. Schladt, Thomas D., et al. "Synthesis and bio-functionalization of magnetic nanoparticles for medical diagnosis and treatment." Dalton Transactions 40.24 (2011): 6315-6343.
12. Cheong, Soshan, et al. "Synthesis and stability of highly crystalline and stable iron/iron oxide core/shell nanoparticles for biomedical applications." ChemPlusChem 77.2 (2012): 135-140.

13. Campbell, Robert B. "Battling tumors with magnetic nanotherapeutics and hyperthermia: turning up the heat." Nanomedicine 2.5 (2007): 649-652.
14. Ikwegbue PC, Masamba P, Oyinloye BE, Kappo AP. Roles of Heat Shock Proteins in Apoptosis, Oxidative Stress, Human Inflammatory Diseases, and Cancer. Pharmaceuticals (Basel). 2017 Dec 23;11(1):2. doi: 10.3390/ph11010002.
15. Li, Q., Lan, P. Activation of immune signals during organ transplantation. Sig Transduct Target Ther 8, 110 (2023). https://doi.org/10.1038/s41392-023-01377-9.
16. Seclì, L., Fusella, F., Avalle, L. et al. The dark-side of the outside: how extracellular heat shock proteins promote cancer. Cell. Mol. Life Sci. 78, 4069–4083 (2021). https://doi.org/10.1007/s00018-021-03764-3
17. Mohan, H.; Mohandoss, S.; Prakash, A.; Balasubramaniyan, N.; Loganathan, S.; Assadi, A.A.; Khacef, A. Cold Plasma Assisted Synthesis of Spinel-CoFe2O4 Nanoparticle with Narrow Bandgap and High Magnetic Activity. Inorg. Chem. Commun. 2024, 167, 12754.
18. Eirini Myrovali, Kyrillos Papadopoulos, Georgia Charalampous, Paraskevi Kesapidou, George Vourlias, Thomas Kehagias, Makis Angelakeris, Ulf Wiedwald, Toward the Separation of Different Heating Mechanisms in Magnetic Particle Hyperthermia, ACS Omega, 12955, EP 12967, 8, 14, American Chemical Society, (2023), doi: 10.1021/acsomega.2c05962.
19. Nain, Sandeep and Kumar, Neeraj and Avti, Pramod Kumar and Chudasama, Bhupendra, The SLP Estimation of the Nanoparticle Systems Using Size-Dependent Magnetic Properties for the Magnetic Hyperthermia Therapy. Journal of Magnetism and Magnetic Materials Volume 565, (2023), 170219, doi.org/10.2139/ssrn.4221744.
20. Philip, John. "Magnetic nanofluids (Ferrofluids): Recent advances, applications, challenges, and future directions." Advances in Colloid and Interface Science 311 (2023): 102810.
21. Pinheiro, Ivanei F.; Brollo, Maria E. F.; Bassani, Gabriel S. ; Varet, Guillaume, Merino-Garcia, Daniel ; Guersoni, Vanessa C. B. ; Knobel, Marcelo ; Bannwart, Antonio C. ; Muraca,; van der Geest, Charlie , Effect of viscosity and colloidal stability on the magnetic hyperthermia of petroleum-based nanofluids, Fuel, Volume 331, id.125810 (2023).
22. Deatsch, Alison E., and Emily E. Evans. "Heating efficiency in magnetic nanoparticle hyperthermia." Journal of Magnetism and magnetic Materials 354 (2014): 163-172.
23. Rosensweig, Ronald E. "Heating magnetic fluid with alternating magnetic field." Journal of magnetism and magnetic materials 252 (2002): 370-374.
24. Hergt, Rudolf, et al. "Magnetic particle hyperthermia: Nanoparticle magnetism and materials development for cancer therapy." Journal of Physics: Condensed Matter 18.38 (2006): S2919.
25. Fannin, Paul C. "Magnetic spectroscopy as an aide in understanding magnetic fluids." Ferrofluids: Magnetically Controllable Fluids and Their Applications. Berlin, Heidelberg: Springer Berlin Heidelberg, 2002. 19-32.
26. Wildeboer, R. R., P. Southern, and Q. A. Pankhurst. "On the reliable measurement of specific absorption rates and intrinsic loss parameters in magnetic hyperthermia materials." Journal of Physics D: Applied Physics 47.49 (2014): 495003.
27. Maria E. F. BrolloIvanei F. PinheiroGabriel S. BassaniGuillaume VaretVanessa C. B. GuersoniMarcelo KnobelAntonio C. BannwartDiego Muraca*Charlie van der Geest, Iron Oxide Nanoparticles In a Dynamic Flux: Implications for Magnetic Hyperthermia-controlled Fluid Viscosity, Journal of Technology & Science,: Health and Medicine(2022).
28. Molcan, M.,. "Magnetic hyperthermia study of magnetosome chain systems in tissue-mimicking phantom." Journal of molecular liquids 320 (2020): 114470.
29. Skumiel, Andrzej, Tomasz Hornowski, and A. Józefczak. "Heating characteristics of transformer oil-based magnetic fluids of different magnetic particle concentrations." International Journal of Thermophysics 32 (2011): 876-885.
30. Musiał, Jakub, Andrzej Skumiel, and Rafał Bielas. "Study of the calorimetric effect in ferrogels subjected to the high-frequency rotating magnetic field." Journal of Magnetism and Magnetic Materials 588 (2023): 171462.
31. Skumiel, Andrzej, "The influence of magnetic nanoparticle concentration with dextran polymers in agar gel on heating efficiency in magnetic hyperthermia." Journal of Molecular Liquids 304 (2020): 112734.
32. Chen, Siyu, and Decai Li. "Control of magnetic particle size in ferrofluid and its effect on rheological properties." Chinese Journal of Mechanical Engineering 35.1 (2022): 79.
33. Molcan, M.,. "Magnetic hyperthermia study of magnetosome chain systems in tissue-mimicking phantom." Journal of molecular liquids 320 (2020): 114470.
34. Myrovali, Eirini, Papadopoulos, Kyrillos, Charalampous, Georgia, Kesapidou, Paraskevi, Vourlias, George, Kehagias, Thomas, Angelakeris, Makis, Toward the Separation of Different Heating Mechanisms in Magnetic Particle Hyperthermia, ACS Omega, (2023), 12955 VL 8 IS 14.
35. Cabrera, David, et al. "Influence of the aggregation, concentration, and viscosity on the nanomagnetism of iron oxide nanoparticle colloids for magnetic hyperthermia." Journal of Nanoparticle Research 17.3 (2015): 121.
36. Elarbaoui, Soumaya. "Magnetite nanoparticles (Fe3O4 NPs) performed by the co-precipitation and green synthesis processes" Main Group Metal Chemistry, vol. 47, no. 1, 2024, pp. 20230029. https://doi.org/10.1515/mgmc-2023-0029

37. Ruíz-Baltazar, Alvaro, et al. "Effect of the surfactant on the growth and oxidation of iron nanoparticles." Journal of nanomaterials 2015.1 (2015): 240948.
38. A.M. Jubb, H.C. Allen, Vibrational spectroscopic characterization of hematite, maghemite and magnetite thin films produced by vapor deposition, Applied materials and interfaces 2 (2010) 2804-2812.
39. Testa-Anta, Martín, et al. "Raman spectroscopy to unravel the magnetic properties of iron oxide nanocrystals for bio-related applications." Nanoscale Advances 1.6 (2019): 2086-2103.
40. Sahoo Y., Goodarzi A., Swihart M.T., Ohulchanskyy T.Y., Kaur N., Furlani E.P., Prasad P.N.,"Aqueous Ferrofluid of Magnetite Nanoparticles: Fluorescence Labeling and Magnetophoretic Control" J. Phys. Chem. B, 109 (2005) 3879-3885.
41. Kumar A, Dixit CK. Methods for characterization of nanoparticles. In: Advances in nanomedicine for the delivery of therapeutic nucleic acids. Elsevier; 2017. p. 43–58.
42. Nguyen, M.D.; Tran, H.-V.; Xu, S.; Lee, T.R. Fe3O4 Nanoparticles: Structures, Synthesis, Magnetic Properties, Surface Functionalization, and Emerging Applications. Appl. Sci. 2021, 11, 11301. https://doi.org/10.3390/app112311301
43. Hadadian, Yaser, "From low to high saturation magnetization in magnetite nanoparticles: the crucial role of the molar ratios between the chemicals." ACS omega 7.18 (2022): 15996-16012.
44. Daoush, Walid M. "Co-precipitation and magnetic properties of magnetite nanoparticles for potential biomedical applications." J. Nanomed. Res 5.3 (2017): 00118.
45. E.A. Perigo, G. Hemery, O. Sandre, D. Ortega, E. Garaio, F. Plazaola, et al., Fundamentals and advances in magnetic hyperthermia, Appl. Phys. Rev. 2 (4), (2015) 041302.
46. T.R. Oliveira, et al., Magnetic fluid hyperthermia for bladder cancer: A preclinical dosimetry study, Int. J. Hyperthermia 29 (8) (2013) 835–844.
47. S. -Y. Wang, S. Huang and D. -A. Borca-Tasciuc, "Potential Sources of Errors in Measuring and Evaluating the Specific Loss Power of Magnetic Nanoparticles in an Alternating Magnetic Field," in IEEE Transactions on Magnetics, vol. 49, no. 1, pp. 255-262, Jan. 2013, doi: 10.1109/TMAG.2012.2224648.
48. Ring HL, Sharma A, Ivkov R, Bischof JC. The impact of data selection and fitting on SAR estimation for magnetic nanoparticle heating. Int J Hyperthermia. 2020 Dec;37(3):100-107. doi: 10.1080/02656736.2020.1810332.
49. Hergt R., Dutz S. Magnetic Particle Hyperthermia—Biophysical Limitations of a Visionary Tumour Therapy. J. Magn. Magn. Mater. 2007;311:187–192. doi: 10.1016/j.jmmm.2006.10.1156.
50. Anand Bhardwaj; Kinnari Parekh, Auto tunable hyperthermic response of temperature sensitive magnetic fluid in agarose gel containing Mn1−xZnxFe2O4 nanoparticles, Journal of Alloys and Compounds, 2024-03, DOI: 10.1016/j.jallcom.2023.173407, ISSN: 0925-8388.
51. Ângela Leão Andrade, Luis Carlos Duarte Cavalcante, José Domingos Fabris Magnetically induced heating by iron oxide nanoparticles dispersed in liquids of different viscosities, Ceramics International 46 (2020) 21496–2150.
52. Tong, S.; Quinto, C.A.; Zhang, L.; Mohindra, P.; Bao, G. Size-Dependent Heating of Magnetic Iron Oxide Nanoparticles. ACS Nano 2017, 11, 6808–6816.
53. Cervadoro, A.; Giverso, C.; Pande, R.; Sarangi, S.; Preziosi, L.; Wosik, J.; Brazdeikis, A.; Decuzzi, P. Design Maps for the Hyperthermic Treatment of Tumors with Superparamagnetic Nanoparticles. PLoS ONE 2013, 8, e57332.
54. Cassim, S.M.; Giustini, A.J.; Baker, I.; Hoopes, P.J. Development of novel magnetic nanoparticles for hyperthermia cancer therapy. Energy-Based Treat. Tissue Assess. VI 2011, 7901, 365–374.
55. Kandasamy, G.; Maity, D. Recent advances in superparamagnetic iron oxide nanoparticles (SPIONs) for in vitro and in vivo cancer nanotheranostics. Int. J. Pharm. 2015, 496, 191–218.
56. Shi, D.; Sadat, M.E.; Dunn, A.W.; Mast, D.B. Photo-fluorescent and magnetic properties of iron oxide nanoparticles for biomedical applications. Nanoscale 2015, 7, 8209–8232.
57. Elbeshir, E.I.A., On the gum arabic to improve the thermal properties of Fe3O4 nanoparticles. AIP Advances, 11(4): 045224.(2021).